Transonic Relief in Fans and Compressors

Demetrios Lefas
Whittle Laboratory,
University of Cambridge,
Cambridgeshire CB3 0DY, UK
e-mail: dl467@cam.ac.uk

Robert J. Miller
Whittle Laboratory,
University of Cambridge,
Cambridge CB3 0DY, UK
e-mail: rjm76@cam.ac.uk

Every supersonic fan or compressor blade row has a streamtube, the "sonic streamtube," which operates with a blade relative inlet Mach number of one. A key parameter in the design of the "sonic streamtube" is the area ratio between the blade throat area and the upstream passage area, A_{throat}/A_{inlet}. In this article, it is shown that one unique value exists for this area ratio. If the area ratio differs, even slightly, from this unique value, then the blade either chokes or has its suction surface boundary layer separated due to a strong shock. Therefore, it is surprising that in practice designers have relatively little problem designing blade sections with an inlet relative Mach number close to unity. This article shows that this occurs due to a physical mechanism known as "transonic relief." If a designer makes a mistake and designs a blade with a "sonic streamtube," which has the wrong area ratio, then "transonic relief" will self-adjust the spanwise streamtube height automatically moving it toward the unique optimal area ratio, correcting for the designer's error. Furthermore, as the blade incidence changes, the spanwise streamtube height self-adjusts, moving the area ratio toward its unique optimal value, effectively controlling the blade's incidence range. Without "transonic relief," supersonic and transonic fan and compressor design would be impossible. This article develops a simple model that allows "transonic relief" to be decoupled from other mechanisms and to be systematically studied. The physical mechanism on which it is based is thus determined and a universal relationship for core compressor preliminary blade design is presented. Finally, its implications in relaxing manufacturing tolerances and in the design of future distortion tolerant blades are discussed. [DOI: 10.1115/1.4052755]

Keywords: compressor stall, surge, and operability, computational fluid dynamics (CFD), fan, compressor, and turbine aerodynamic design, fluid dynamics and heat transfer phenomena in compressor and turbine components of gas turbine engines, turbomachinery blading design, inlet flow distortion, manufacturing

1 Introduction

It is well known that as the inlet Mach number to a two-dimensional cascade of blades approaches unity design of the blade row becomes increasingly difficult, as demonstrated by McKenzie [1] and Cumpsty [2]. As the inlet Mach number rises toward unity, the operating incidence range of the blade row reduces dramatically. On the negative incidence side, this is because the blade row chokes. On the positive incidence side, this is because a sonic patch terminates in a strong shock, which causes the suction surface boundary layer to separate. Ginder and Calvert [3] conclude that this makes the design of two-dimensional or quasi-three-dimensional transonic compressors and fans "quite challenging" and the design of a two-dimensional cascade at an inlet Mach number of one "a near impossibility."

Wright and Miller [4] used experimental data from NASA high-speed compressor stages to develop a correlation for the design of two-dimensional transonic blade sections.

They postulated that the key parameter in the design is the area ratio between the throat of the blade and the upstream passage $A_{\text{throat}}/A_{\text{inlet}}$. Section 3 shows that for the "sonic streamtube," i.e., the streamtube with an inlet Mach number of one, only one unique value of this area ratio exists, as shown in Fig. 1(*a*). If the area ratio deviates from this value, then the blade is either choked

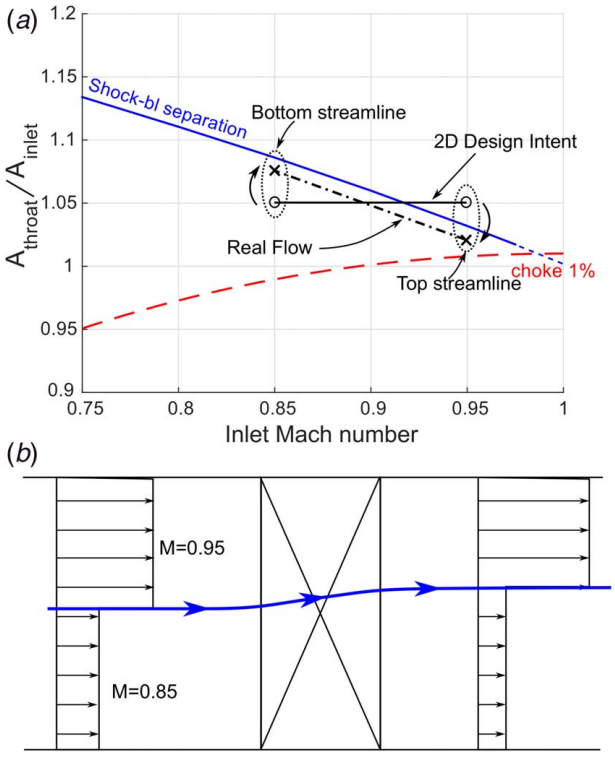

Fig. 1 Illustration of transonic relief using a simple model

Contributed by the International Gas Turbine Institute (IGTI) of ASME for publication in the Journal of Turbomachinery. Manuscript received July 31, 2021; final manuscript received October 7, 2021; published online November 15, 2021. Tech. Editor: David G. Bogard.

or has its suction surface boundary layer separated due to a strong shock.

In practice, designers have relatively little problem designing blade sections with an inlet Mach number of one. Section 4 shows that this is due to a mechanism the authors termed "transonic relief." This mechanism will be shown to always act to self-adjust the streamtube contraction, so that as the inlet Mach number approaches unity, the streamtube area ratio always moves toward the optimum value indicated in Fig. 1(*a*).

Systematically studying transonic relief in real compressors and fans is difficult. This is because the blade speed, and therefore the blade inlet Mach number and flow angle, varies up the span of the blade. This means that the blade design has to vary up the span. As a result, it is difficult to determine whether any streamtube contraction is due to "transonic relief" or due to variations in the blade design.

Section 4 systematically studies "transonic relief" using the simple model depicted in Fig. 1(*b*). The model involves a rectilinear cascade of blades with an inlet spanwise variation in the Mach number. Because the model is a rectilinear cascade, the blade design can remain constant across its span. The inlet flow to the cascade is modeled as two streams, each with a different Mach number but with the same inlet flow angle. The model, therefore, allows the effects of transonic relief to be studied independently of any other effects.

An example illustrating the effect of transonic relief is shown in Fig. 1. In this case, a uniform blade profile with $A_{throat}/A_{inlet} = 1.05$ has been designed. The top and bottom streams are operating at an inlet Mach number of 0.95 and 0.85, respectively. The black solid line connecting the data points marked by a circle in Fig. 1(*a*) shows the design intent flow conditions of the two streams. It should be noted that the top stream has been deliberately designed at too high a value of A_{throat}/A_{inlet}. At this value of A_{throat}/A_{inlet}, the top section of the blade should have its suction surface separated by a strong shock.

The crosses and dot-dashed line in Fig. 1(*a*) show the real flow conditions of the two streams extracted from the computational fluid dynamics (CFD) later in this article. Transonic relief can be seen to contract the top streamtube and expand the bottom streamtube, moving the higher Mach number streamtube to $A_{throat}/A_{inlet} = 1.015$. This is close to the optimal value of $A_{throat}/A_{inlet} = 1.01$. This results in the blade operating without separation or choke across its entire span.

In this article, it will be demonstrated that transonic relief always acts to move A_{throat}/A_{inlet} toward the optimal value of 1.01. It will be shown that as the Mach number approaches unity, the strength of the transonic relief mechanism increases. In fact, in the case where the blade is designed with too low a value of A_{throat}/A_{inlet}, where it should be choked, transonic relief will be shown to expand the streamtube, thus once again moving A_{throat}/A_{inlet} toward the optimal value of 1.01. Finally, this article discusses the design implications of transonic relief.

2 Methodology

The MISES [5] CFD code was employed in all two-dimensional and quasi-three-dimensional designs studied. MISES is a quasi-3D Euler code with a coupled boundary layer solver. The blades were represented in two dimensions, but variations in streamtube height in the spanwise direction could be introduced. The turbulence intensity was specified in the code as typically found in compressors (Tu = 4%) and was run at a Reynolds number of one million. Boundary layer transition was triggered at the leading edge on both the pressure and suction surfaces. It should be noted that MISES has been extensively calibrated against experiments for transonic compressors [6].

The three-dimensional CFD solutions presented were all computed using TURBOSTREAM. It is a structured multiblock Reynolds-averaged Navier–Stokes solver based on TBLOCK and implemented for parallel GPU operation. Further details and validation are presented in Ref. [7]. The turbulence model used was the Spalart-Allmaras [8]. The meshing process was automated using AUTOGRID. A y^+ lower than one was ensured at every blade surface, and a mesh sensitivity study was performed for every case considered. Transition was not modeled, and the code considers the flow to be fully turbulent.

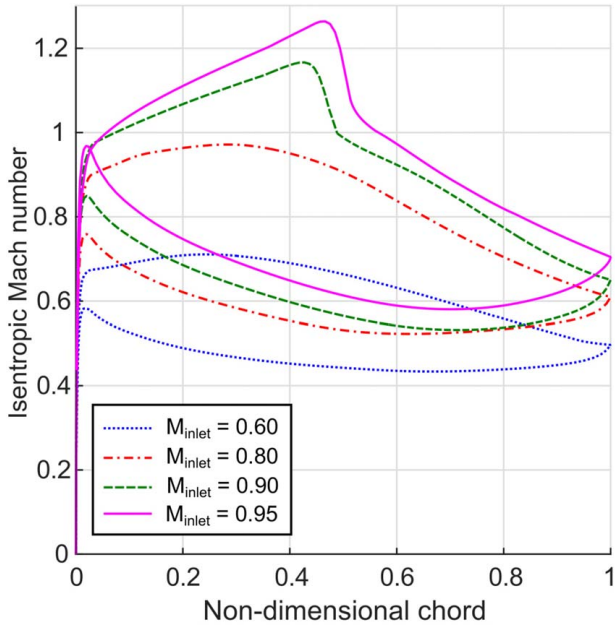

Fig. 2 Isentropic Mach number profiles of blades operating at $M_{inlet} = 0.60, 0.80, 0.90, 0.95$

All blades were designed for the same duty (flow coefficient, loading, and reaction) typical of modern transonic compressor/fan sections. At an inlet Mach number of 0.90 and an inlet flow angle of 52 deg, without any streamtube contraction, this resulted in a total airflow turning of 14 deg at design.

In addition, the blades were all designed to the same aerodynamic standards. In particular, all designs put the stagnation streamline on the nose of the blade (i.e., zero local incidence). The shape factor of the boundary layer at the trailing edge of the suction surface was fixed. The blades were designed with a "linear shape factor philosophy," where the suction surface shape factor increased linearly from the location of peak suction, or the location of the shock, to the trailing edge. The pre-shock Mach number was limited to values that would not cause premature boundary layer separation. The pressure distributions away from the shock were maintained as smooth. The Mach number distributions of blades designed at an inlet Mach number of 0.60, 0.80, 0.90, and 0.95 are depicted in Fig. 2.

3 Key Design Parameter A_{throat}/A_{inlet}

In this section, the streamtube contraction was deliberately held constant at a value of unity to systematically study the dependence of transonic compressor performance on the area ratio between the throat of the blade and the upstream passage.

The area ratio can be written geometrically as follows:

$$\frac{A_{throat}}{A_{inlet}} = \frac{o}{s\cos(\alpha_1)} \times AVDR_{throat} \tag{1}$$

where $AVDR_{throat}$ is the axial velocity–density ratio at the throat and is a measure of the streamtube contraction between the throat and the upstream. In this section, the streamtube contraction will be fixed by setting $AVDR_{throat} = 1$, as depicted in Fig. 3.

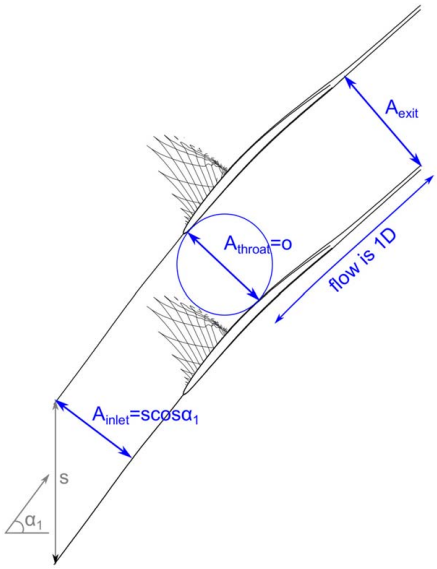

Fig. 3 Important geometric dimensions

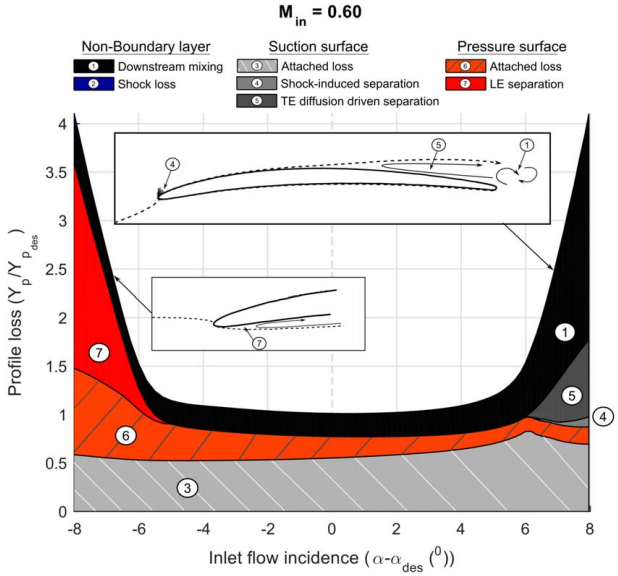

Fig. 5 Loss breakdown of a subsonic Mach number compressor (M_{inlet} = 0.60, 2D spanwise uniform)

3.1 Transonic and Subsonic Flow Physics. Figure 4 shows the variation in operating incidence range of a two-dimensional blade section with Mach number. As the relative inlet Mach number of a compressor blade increases, the operating incidence range of the compressor decreases. Plots of this type are normally for a fixed blade geometry. In Fig. 4, the geometry of the blade has been specifically optimized at each inlet Mach number.

The two black lines in Fig. 4 show the incidence range at which the loss rises to 25% above the design incidence loss. The red line demonstrates the "real" choke line, which is extracted from the CFD. The transonic regime is defined as the region of the blade in which a supersonic patch exists at the design incidence and is marked in green.

It can be deduced that the negative incidence range of the blade starts to close up at Mach numbers above 0.50. This occurs because, even though the blade is entirely subsonic at design incidence, at sufficiently high negative incidence it develops a supersonic patch on the leading edge pressure surface.

To understand the variation of incidence range with Mach number, it is necessary to examine the loss mechanisms responsible.

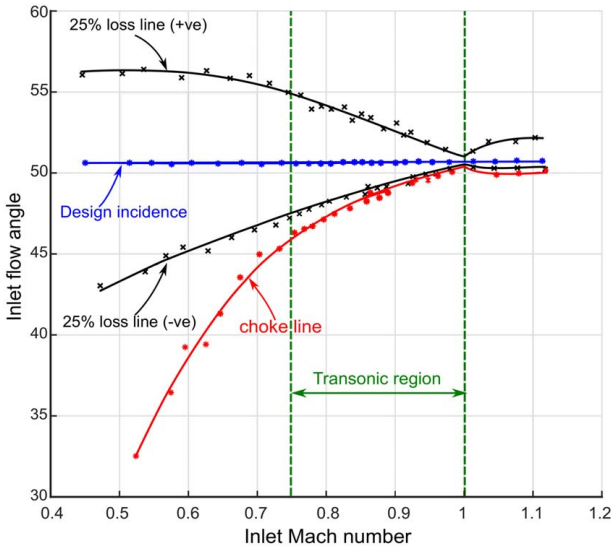

Fig. 4 Mach number against incidence plot for "well-designed" blades at that Mach number (2D spanwise uniform)

A decomposition of the loss mechanisms at a subsonic (M_{inlet} = 0.60) and transonic (M_{inlet} = 0.90) inlet Mach number is presented in Figs. 5 and 6, respectively.

The subsonic case is shown in Fig. 5. The positive incidence range limit is controlled by a sequence of connected loss mechanisms. Considering the rise in loss for incidence above about 6 deg; at the leading edge, a small shock occurs, but this shock is weak and creates very little loss; however, it causes the boundary layer to separate causing a small separation bubble (4). This loss increases the thickness of the suction surface boundary layer and results in the turbulent boundary layer separating upstream of the trailing edge (5). Finally, this causes a thickening of the wake and raises the downstream mixing loss (1). Therefore, it is clear that even at this subsonic Mach numbers, the positive incidence range is shock dependent, and even though the shock produces little loss, it sets off a cascade of loss mechanisms, which results in a reduction of the blade's positive incidence range.

The negative incidence range is controlled by a leading edge separation (7), which results in a rapid rise in loss due to mixing in the separated shear layer in the blade passage (6), (7), and downstream of the blade row (1). It should be noted that this rise in loss occurs at a negative incidence, which is lower in magnitude than the negative incidence at which the blade row chokes. The difference in the incidence at which loss rises and at which choke occurs can be observed in Fig. 4.

The transonic case (M_{inlet} = 0.90) is shown in Fig. 6. The shock that terminates the supersonic bubble on the suction surface is now responsible for a significant amount of loss (2) even at zero incidence. At a positive incidence of 0.5 deg, the peak Mach number reaches a value of M_{peak} = 1.29 and the suction surface boundary layer separates (4) but reattaches to form a separation bubble. At positive incidences above 3.5 deg, the separated boundary layer no longer reattaches, and the suction surface remains separated up to the trailing edge (with a jump in loss mechanism (4)). This significantly increases loss due to mixing in the separation and the downstream wake (1).

It is clear that the loss mechanisms responsible for the positive incidence range significantly differ between subsonic and transonic Mach number regimes. In both regimes, a sonic bubble limits the positive incidence range, but at M_{inlet} = 0.60 the final suction surface separation at high incidence is driven by deceleration toward the rear of the blade; while at M_{inlet} = 0.90, the separation is caused by the shock. This change in separation mechanism is

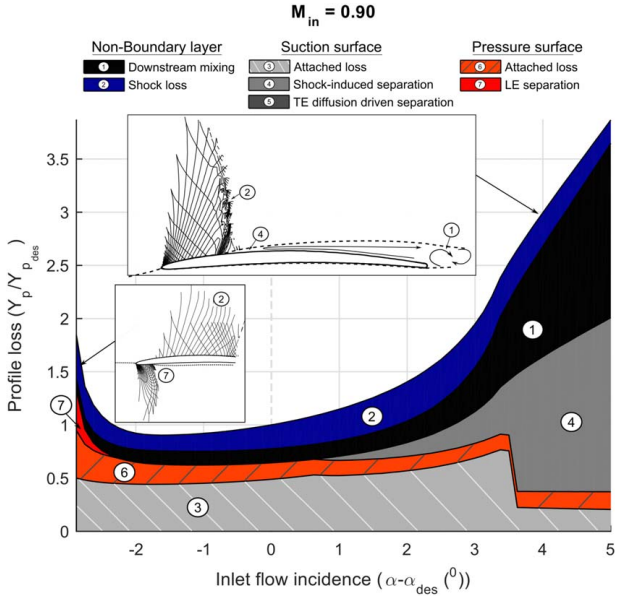

Fig. 6 Loss breakdown of a transonic Mach number compressor ($M_{inlet} = 0.90$, 2D spanwise uniform)

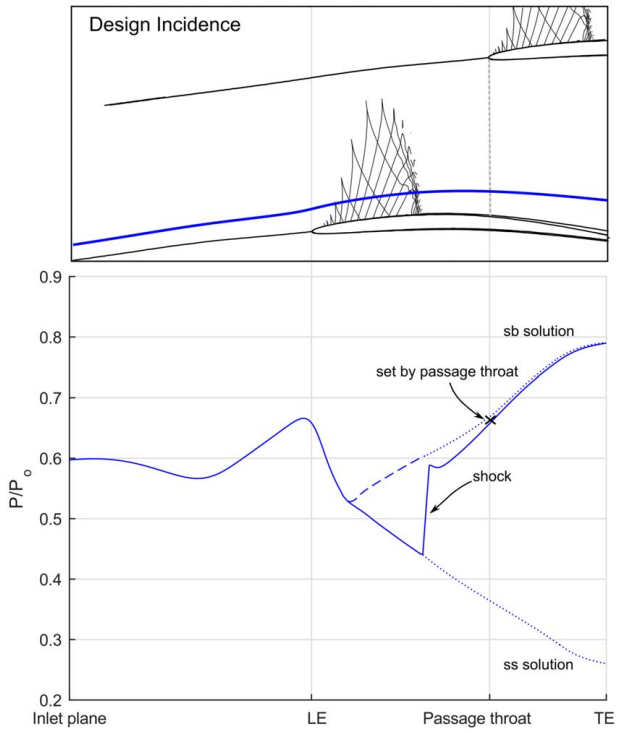

Fig. 7 Single streamline in the transonic region of the blade ($M_{inlet} = 0.90$, zero incidence and constant streamtube height)

responsible for the reduction in positive incidence range shown in Fig. 4 at inlet Mach numbers greater than approximately 0.75.

At negative incidence, the transonic case shown in Fig. 6 shows a rise in loss at incidences below −2.0 deg. This is caused by a shock-induced leading edge separation (7), which occurs at an incidence that is very close to the choking incidence (−2.8 deg). This differs from the subsonic case, where the leading edge separation is not caused by a shock.

To sum up, the major difference between the transonic case and the subsonic case is that in the transonic case, both the negative and positive incidence ranges are entirely shock driven.

3.2 Physical Importance of A_{throat}/A_{inlet}. The flow field in the transonic region of the blade at an inlet Mach number of 0.90 is shown in Fig. 7 for zero incidence. As shown in the upper plot, there is a supersonic patch on the suction surface terminated by a shock that is not strong enough to separate the boundary layer. The blue line in the upper diagram is a streamline 15% across the pitch from the stagnation streamline at inlet. The static pressure along this streamline is illustrated in the lower plot.

Upstream of the blade leading edge the flow can be seen to decelerate due to the presence of the blade depicted below it. The flow then accelerates around the leading edge and over the suction surface, becoming supersonic. The supersonic patch is terminated by a shock, which causes a sudden rise in pressure. It then decelerates subsonically to the trailing edge, increasing to the exit pressure. The two dotted blue lines show the subsonic and supersonic solutions to the compressible flow equations. These are the lines that the pressure distribution would follow if the flow were entirely subsonic or supersonic. The vertical distance between the subsonic and supersonic solutions determines the shock strength.

The physical importance of A_{throat}/A_{inlet} is shown in Fig. 8. This figure depicts three streamlines passing through the blade passage. The green streamline almost avoids the shock and is isentropic. It has a very small sonic patch, which ends with an isentropic expansion. However, the red and blue streamlines are not isentropic and pass through a shock at the end of the sonic region.

The cross marked in Fig. 8 shows that at the throat, the ratio of static and stagnation pressure is the same on all three streamlines. Because the shock is relatively weak, the variation in stagnation pressure across the throat is small. This means that the static pressure is uniform across the throat.

The uniformity of the static pressure can also be inferred from the curvature of the three streamlines in Fig. 8. Upstream of the throat, the streamlines can be seen to be curved. However, from the throat

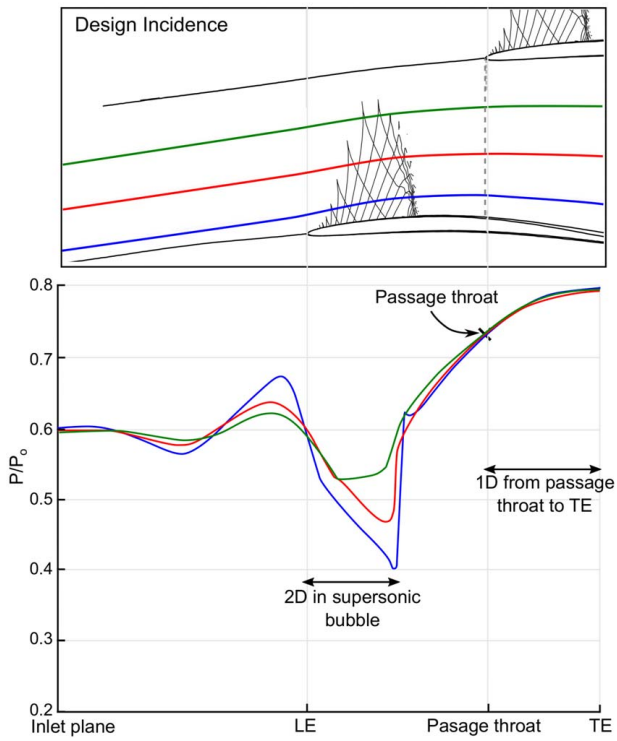

Fig. 8 Three streamlines in the transonic region of the blade ($M_{inlet} = 0.90$, zero incidence and constant streamtube height)

downstream, they can be seen to be straight and divergent. This shows that from the throat to the suction surface trailing edge, the flow simply undergoes a one-dimensional diffusion. The fact that the static pressure is uniform at the throat is not intuitive but was observed to be the case in all the transonic blades studied.

Because the pressure at the geometric throat and at the inlet of the blade row is uniform and because the two regions are linked by the green isentropic streamline, the pressure at the throat becomes fixed by A_{throat}/A_{inlet} alone. It is for this reason that the geometric parameter A_{throat}/A_{inlet} plays such an important role in the design of transonic blade rows.

3.3 The Universal Nature of A_{throat}/A_{inlet}. The effect of varying A_{throat}/A_{inlet}, while holding the inlet Mach number at 0.90, is studied first and is depicted in Figs. 9 and 10. To achieve this, the pitch-to-chord of the blade row is held constant, and the camber distribution is changed while keeping the maximum thickness of the blade constant.

As discussed in Sec. 3.2, altering A_{throat}/A_{inlet} changes the pressure at the throat location, shown in Fig. 9. The shock remains in the same location, but its strength changes. The effect of raising A_{throat}/A_{inlet} is therefore simply to raise the shock strength. The effect is also evident in the isentropic blade Mach number distributions presented in Fig. 10.

The effect of changing the blade row's pitch-to-chord while keeping A_{throat}/A_{inlet} constant is shown in Figs. 11 and 12. These cases are important to showcase that the strength of the shock is independent of a blade row's pitch-to-chord and the blade geometry up to the throat. The isentropic Mach number plots, presented in Fig. 11, show that as the pitch-to-chord is raised, the location of the shock moves rearward, but the strength of the shock remains unchanged.

The geometric effect of removing blades is that the passage throat area moves further downstream. In Fig. 11, the passage throat location on the blade's suction surface is also marked with crosses. It can be seen that there is little to no variation in the isentropic Mach number at the throat location since A_{throat}/A_{inlet} has been kept constant.

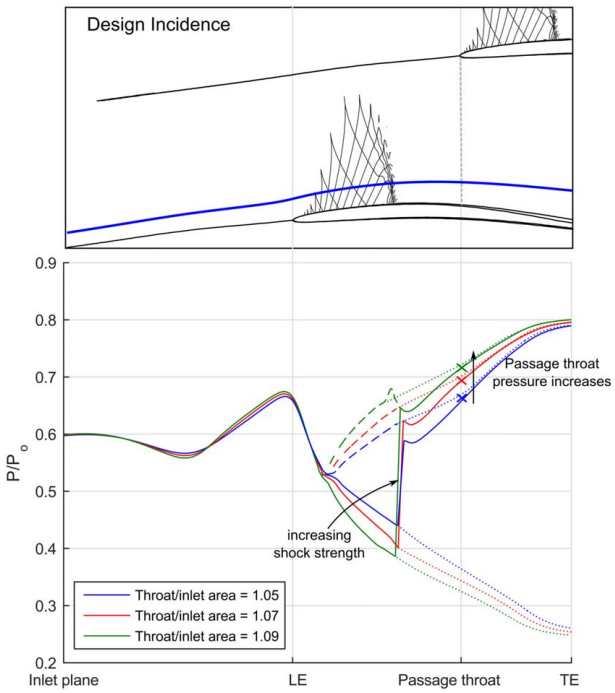

Fig. 9 Effect of varying A_{throat}/A_{inlet} ($M_{inlet} = 0.90$, $s/c = 0.90$, zero incidence and constant streamtube height)

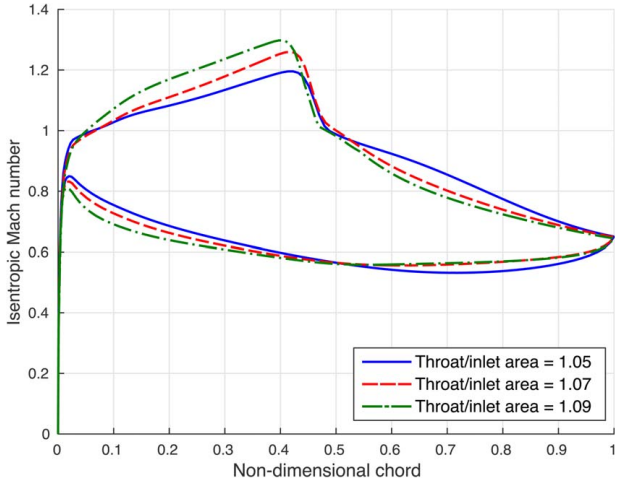

Fig. 10 Effect of varying A_{throat}/A_{inlet} on blade isentropic Mach number ($M_{inlet} = 0.90$, $s/c = 0.90$, zero incidence and constant streamtube height)

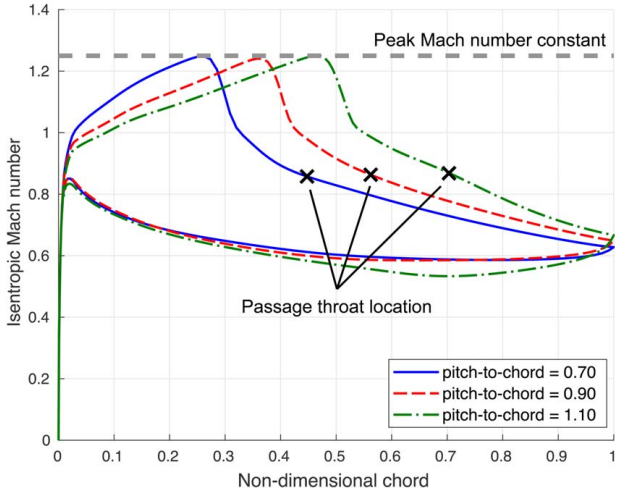

Fig. 11 Effect of varying pitch-to-chord on blade isentropic Mach number ($M_{inlet} = 0.90$, $A_{throat}/A_{inlet} = 1.05$, zero incidence and constant streamtube height)

In Fig. 12, the streamwise distance (plotted on the x-axis) has been scaled linearly by dividing the streamwise distance by the distance between the inlet and the passage throat. This causes the passage throat and shock location for the three cases to collapse. It is clear from Fig. 12 that pitch-to-chord does not affect the strength of the shock because the passage throat pressure remains constant.

To demonstrate the universal nature of A_{throat}/A_{inlet}, Fig. 13 plots the relationship for blades of different pitch-to-chord, thickness, streamtube contraction, and loading. This figure shows that in the transonic regime, the ratio A_{throat}/A_{inlet} alone sets the flow field in the blade.

3.4 Dependence of Operating Range on A_{throat}/A_{inlet}. The effect of A_{throat}/A_{inlet} on the operating range of the blade row at Mach 0.90 is shown in Fig. 14. The blades are designed at a constant pitch-to-chord and maximum thickness, but the camber distribution has been changed to vary the area ratio.

The red and black lines in Fig. 14 illustrate the effect of changing A_{throat}/A_{inlet} on the suction surface shock strength for the case of +2 deg and design incidence, respectively. The cause of this effect at positive incidence is shown in Fig. 15, which illustrates

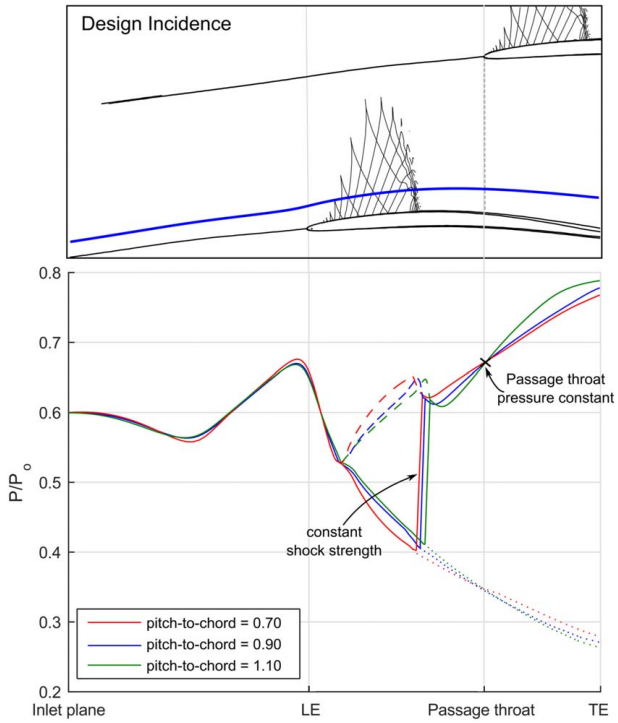

Fig. 12 Effect of varying pitch-to-chord ($M_{inlet} = 0.90$, $A_{throat}/A_{inlet} = 1.05$, zero incidence and constant streamtube height; plot scaled to keep passage throat location fixed)

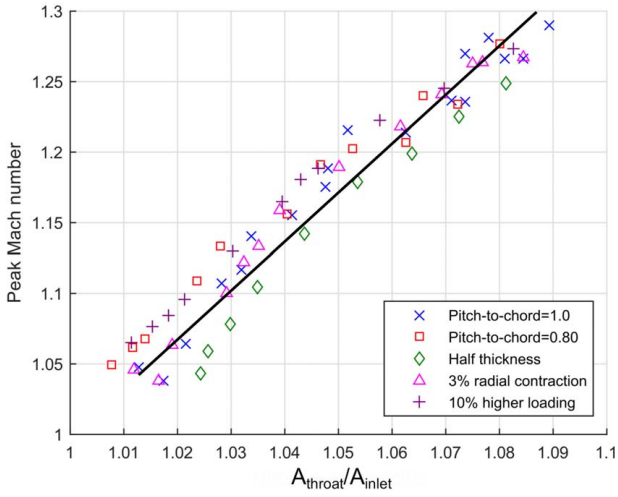

Fig. 13 Variation of peak Mach number with A_{throat}/A_{inlet} ($M_{inlet} = 0.90$ and zero incidence)

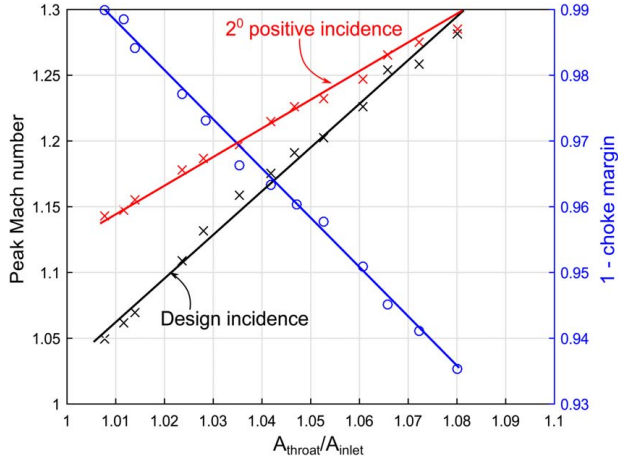

Fig. 14 Dependence of positive and negative incidence range on A_{throat}/A_{inlet} ($M_{inlet} = 0.90$, $s/c = 0.90$ and constant spanwise streamtube height)

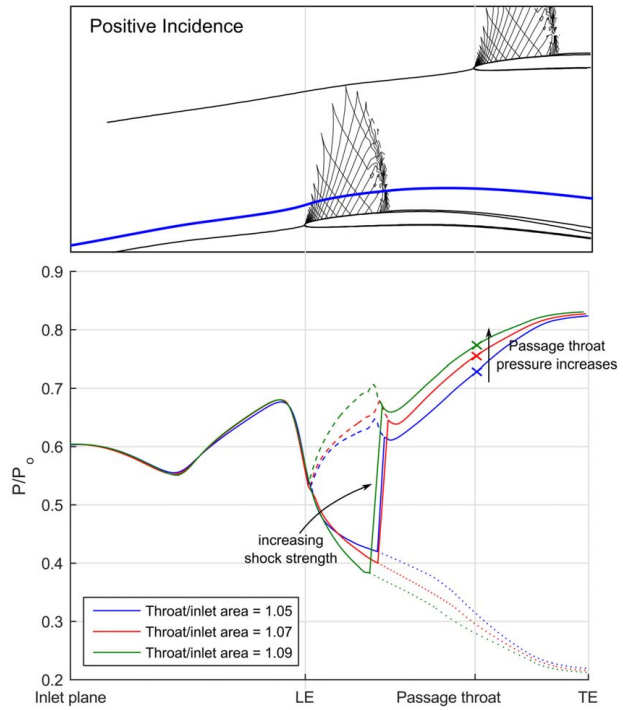

Fig. 15 Effect of varying A_{throat}/A_{inlet} at 2 deg positive incidence ($M_{inlet} = 0.90$, $s/c = 0.90$ and constant spanwise streamtube height)

that as A_{throat}/A_{inlet} is raised, the pressure at the throat increases and thus the shock strength increases. This showcases that raising A_{throat}/A_{inlet} acts to reduce positive incidence range. Conversely, the blue line in Fig. 14 shows the effect of changing A_{throat}/A_{inlet} on the choke margin. This implies that designs with a high A_{throat}/A_{inlet} have a high choke margin.

The effect of A_{throat}/A_{inlet} on the shape of the "loss loop" is depicted in Fig. 16. It can be observed that the minimum design loss occurs over a range of $1.04 < A_{throat}/A_{inlet} < 1.06$. The final choice of A_{throat}/A_{inlet} depends on the exact positive and negative incidence range required by the designer. This can be deduced from Fig. 16. It is clear that over this optimal range, the exact value of A_{throat}/A_{inlet} causes the loss loops to slide from left to right; trading positive incidence range for negative incidence range. The effect of varying A_{throat}/A_{inlet} over a range of Mach numbers can be seen in Fig. 17.

Finally, it is worth noting that as the inlet Mach number is reduced, the effect of A_{throat}/A_{inlet} on the operating range decreases. Figure 18 shows the effect of A_{throat}/A_{inlet} on the "loss loop" at an inlet Mach number of 0.60. It can be seen that varying A_{throat}/A_{inlet} has little effect on the operating range and simply acts to forward-load or rear-load the blade, changing the design loss by around 15%.

3.5 Setting Pitch-to-Chord. The choice of pitch-to-chord of a subsonic blade is often based on diffusion arguments along the rear of the blade suction surface. This is logical for subsonic blades

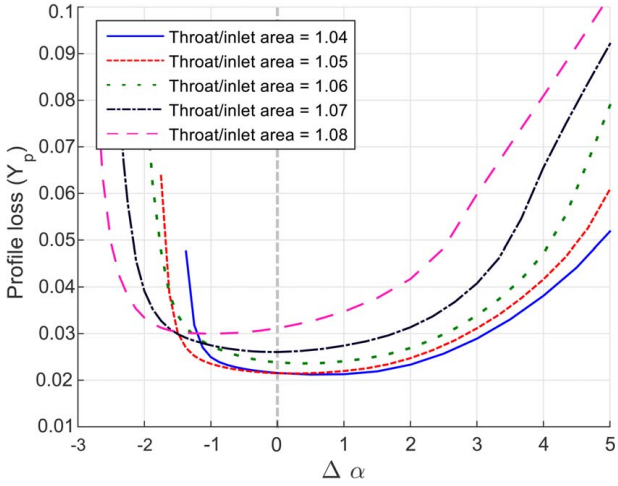

Fig. 16 Dependence of loss loop on A_{throat}/A_{inlet} ($M_{inlet} = 0.90$, $s/c = 0.90$ and constant streamtube height)

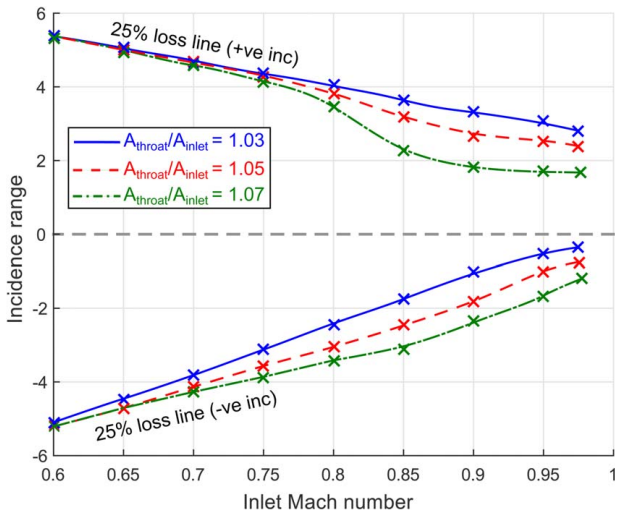

Fig. 17 Incidence range against inlet Mach number dependence on A_{throat}/A_{inlet}

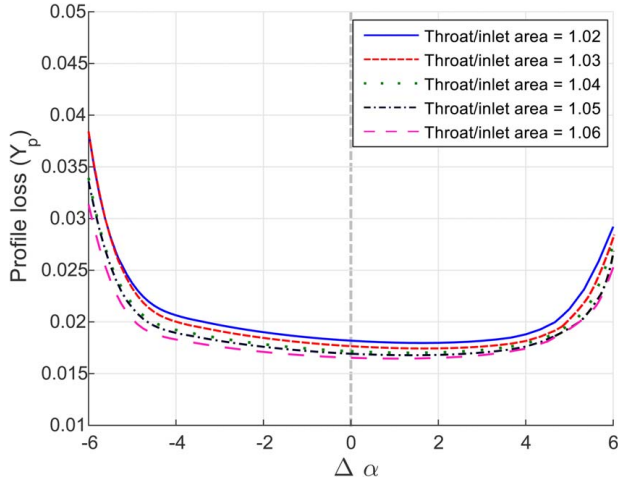

Fig. 18 Dependence of loss loop on A_{throat}/A_{inlet} ($M_{inlet} = 0.60$, $s/c = 0.90$ and constant streamtube height)

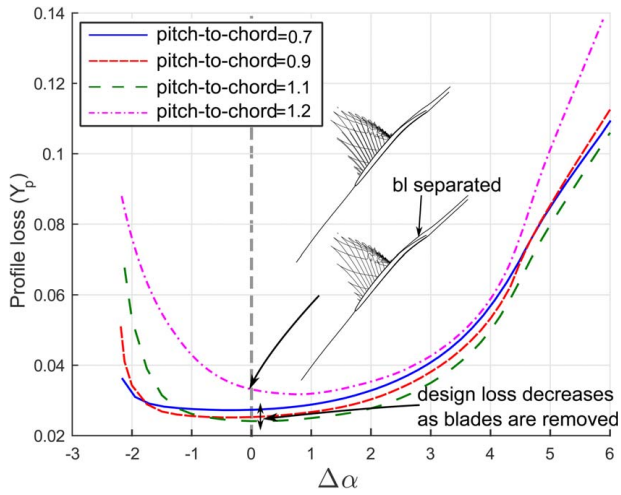

Fig. 19 Dependence of loss loop on pitch-to-chord ($M_{inlet} = 0.90$, $A_{throat}/A_{inlet} = 1.05$ and constant streamtube height)

because the positive incidence range is limited by an adverse pressure gradient separating the suction surface boundary layer. As a result, the pitch-to-chord of a subsonic blade row is selected by either fixing the diffusion factor or the shape factor of the suction surface boundary layer at the trailing edge.

For transonic blades, the positive and negative incidence range is determined by a shock-induced separation with no subsequent reattachment. A new method of setting the pitch-to-chord must therefore be determined and will now be outlined. The effect of varying pitch-to-chord at a constant A_{throat}/A_{inlet} of 1.05 is shown in Fig. 19.

The first point to note is that the positive incidence range is not a strong function of pitch-to-chord. Figure 19 shows that between a pitch-to-chord of 0.7 and 1.1, the width of the loss loop shows little change. This is as expected from the aforementioned arguments presented in this article and demonstrated in Figs. 11 and 12. For fixed A_{throat}/A_{inlet}, the peak Mach number is virtually constant, and it is this that causes the shock-induced separation. However, at pitch-to-chords $\geq$1.20, both the positive and the negative incidence ranges are shown to reduce. The positive incidence range is reduced because the passage throat has moved so close to the trailing edge that there is not sufficient blade surface to successfully diffuse the flow to the exit pressure, and as a result, the boundary layer separates.

The second point to note is that the design loss decreases as the pitch-to-chord rises, provided that the boundary layer has not separated by diffusion close to the trailing edge as outlined previously. This occurs because as the number of blades is reduced, the overall wetted area decreases, thus reducing the design loss.

The negative incidence range reduction is more difficult to understand. Figure 20 shows the effect of raising pitch-to-chord at an incidence of −1.5 deg (close to choking). As pitch-to-chord is raised, the position of the shock on the suction surface moves rearward toward the throat. As the shock approaches the throat, its position becomes locked. This causes the strength of the shock to rise. It should be noted that for most values of pitch-to-chord, and over most of the incidence range, the shock strength is independent of pitch-to-chord, as described in Sec. 3.3. However, at a pitch-to-chord ratio of around 1.20, the shock strength becomes strong enough to separate the suction surface boundary layer. In this case, we are in the strange situation where the negative incidence range is limited by suction surface separation.

In conclusion, a relatively wide range of pitch-to-chords is acceptable in transonic blade design. As shown in Fig. 19, a pitch-to-chord of 0.7 to 1.0 results in blades with a similar operating incidence range. However, if the aim is to minimize design loss, then a pitch-to-chord of 1.0 would be optimal. The weak dependence on pitch-to-chord is fortuitous for a designer as in reality

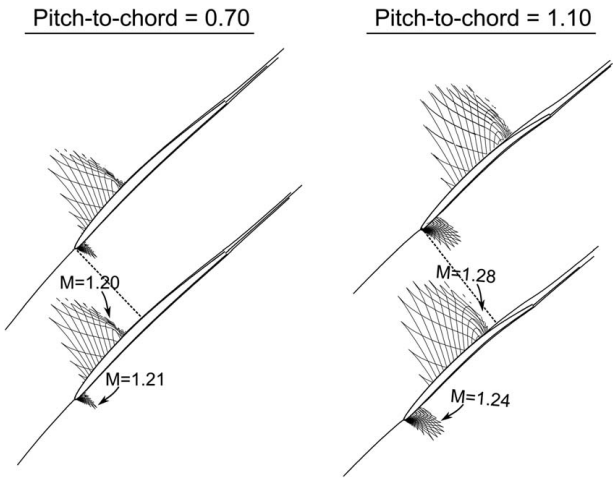

Fig. 20 Effect of pitch-to-chord on shock structure at −1.5 deg incidence (0.5 deg from choking incidence and $M_{inlet} = 0.90$)

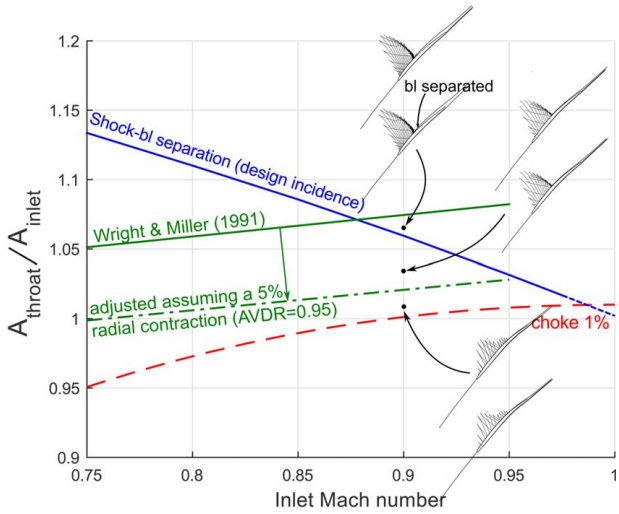

Fig. 21 Limits on profile design as inlet Mach number approaches one

the pitch-to-chord is likely to be set by other parts of the blade design.

3.6 Optimal A_{throat}/A_{inlet} near $M_{inlet} = 1.0$. The restrictions on the blade design as the inlet Mach number approaches unity are shown in Fig. 21. Schematics of the shock structure of different blade designs at an inlet Mach number of 0.90 are also presented. As A_{throat}/A_{inlet} increases, so does the shock strength. The blue line depicts the upper limit at which the design shock strength is enough to cause premature boundary layer separation at each Mach number. It is obtained by applying a best-fit line to a wide range of blade designs at each inlet Mach number (as shown in Fig. 13). The red dashed line shows the lower limit where the blade has a 1% choke margin. The two lines intersect at a Mach number of 0.98 and an $A_{throat}/A_{inlet} = 1.01$. This implies that at an inlet Mach number of 0.98, the blade must have $A_{throat}/A_{inlet} = 1.01$.

To test out the hypothesis, a blade was designed with an inlet Mach number of 0.98 and $A_{throat}/A_{inlet} = 1.01$. This design was very difficult to achieve. The flow field is plotted in Fig. 22. It shows that the peak Mach number on the suction surface produces a shock, which is just strong enough to separate the boundary layer without subsequent reattachment. On the pressure surface near the leading edge, the peak Mach number is 1.08, which means that the blade is very close to choking.

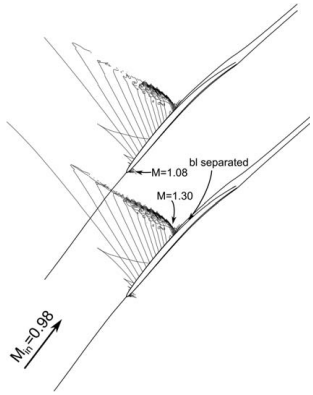

Fig. 22 Highest inlet Mach number at which blade design is possible ($M_{inlet} = 0.98$ and $A_{throat}/A_{inlet} = 1.01$)

This indicates that with a fixed streamtube contraction restriction, as the Mach number increases, it becomes increasingly difficult to design a "good" aerodynamic blade. In fact, at inlet Mach numbers above 0.98, designing a "good" aerodynamic blade becomes practically impossible. In Sec. 4, it will be proven that by the mechanism of transonic relief, this problem is avoided in practice.

3.7 Design Correlation for A_{throat}/A_{inlet}. Figure 21 also shows the existing experimental correlation from Wright and Miller [4]. The correlation is based on individual blade sections up the span of NASA single-stage compressor tests. The highest inlet Mach number section used was 0.90. The correlation gives the variation of $o/s\cos\alpha_1$ at design incidence with inlet Mach number (green solid line). To convert $o/s\cos\alpha_1$ into area ratio, the knowledge of $AVDR_{throat}$ is required as shown in Eq. (1). Unfortunately, the $AVDR_{throat}$ of the transonic blade sections used by Wright and Miller to develop their correlation is not available. In Fig. 21, the correlation of Wright and Miller is plotted assuming an $AVDR_{throat}$ of 1.0.

At first sight, the correlation seems to overpredict the optimum design A_{throat}/A_{inlet}. However, the reason for this is that the true $AVDR_{throat}$ is not accounted for. Axial velocity density ratio (AVDR; $\rho_1 V_{x1}/\rho V_x$) equal to about 0.95 (not unreasonable for high-speed blade rows) would be required for the Wright and Miller correlation to agree with this study. This highlights the importance of using the true area ratio in design and not trusting correlations based on two-dimensional geometric parameters.

The new correlation that can be used in the preliminary design is expressed as follows:

$$\frac{A_{throat}}{A_{inlet}} = 1.1617 - 0.1556 M_{inlet} \tag{2}$$

In translating this back to two-dimensional geometric parameters, it is important that the true $AVDR_{throat}$ in the real machine is used.

4 Transonic Relief

Transonic relief will be studied by performing 3D CFD on a simple model of a rectilinear cascade. This will allow the effect of inlet Mach number and incidence on the magnitude of transonic relief alone to be studied, as the model manages to decouple the radial pressure gradient and variable blade section design effects. The mechanism responsible for transonic relief will then be explained.

4.1 Simple Model. An idealized rectilinear cascade blade will be considered, as shown in Fig. 23. The blade is of uniform

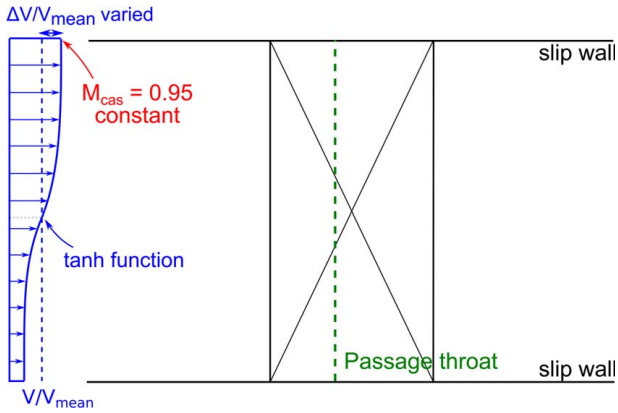

Fig. 23 Idealized cascade with nonuniform inlet

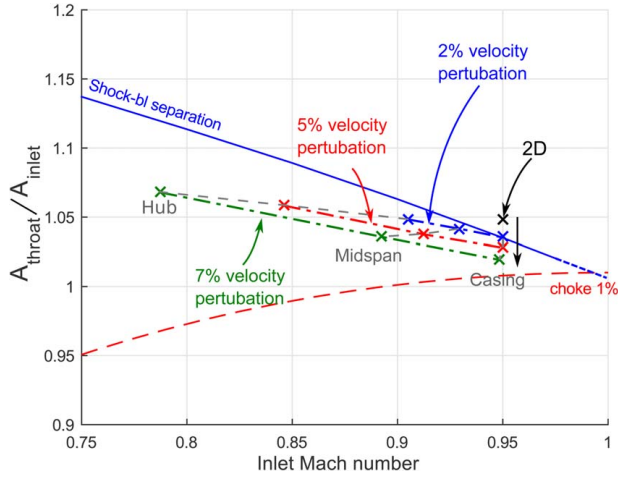

Fig. 24 Spanwise variation in streamtube area ratio (casing Mach number constant at 0.95)

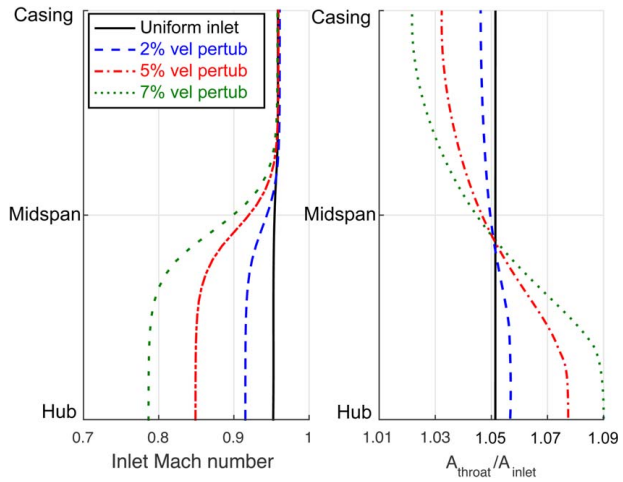

Fig. 25 Spanwise variation in the inlet Mach number profile and streamtube area ratio for a 2%, 5%, and 7% velocity perturbation

geometry up the span and has an aspect ratio of 1.50 with both endwalls modeled as slip walls. The blades are designed with an $A_{throat}/A_{inlet} = 1.05$. As can be deduced from Fig. 21, this area ratio is too high for a blade to operate at Mach numbers above 0.92. The blade row was run at a uniform inlet Mach number of 0.95, and as expected, the suction surface of the blade row separated with a strong shock.

The inlet profile to the cascade is composed of two uniform streams of different Mach numbers. The upper stream (casing streamtube) includes the top third of the passage and has an inlet Mach number of 0.95. As discussed previously, it is impossible for the blade to operate in this condition without its suction surface being separated by a strong shock. The lower stream (hub streamtube) includes the bottom third of the passage and has a variable Mach number. In the middle third of the passage, a hyperbolic tangent variation is used to join the two uniform streams. The variation in inlet Mach number upstream is achieved computationally by setting a uniform total temperature and a variation in total pressure at the inlet.

The virtue of this simple model, over a real annulus of blades with an engine representative inlet, is that the streamtube contraction and the underlying physical mechanism that causes it can be more easily identified and explained.

4.2 Varying Inlet Mach Number. The 3D CFD results for three cases with different lower stream Mach numbers are shown in Fig. 24 as blue, red, and green dashed lines. It is worth noting that these represent small velocity perturbations of 2%, 5%, and 7% of the mean velocity. The black cross, at an area ratio of 1.05 and a Mach number of 0.95, signifies the point at which the blade was designed.

Figure 24 shows that the Mach 0.95 streamtubes, in the top third of the passage, contract and the lower Mach number streamtubes, in the bottom half of the passage expand. The mechanism of transonic relief acts to move the higher Mach number streamtube toward its ideal area ratio. If it were not for this behavior, the suction surface of the blade in the casing region would have separated due to shock boundary layer separation. It will be shown in Sec. 4.4 on the effect of varying incidence that the same effect occurs, but in the opposite direction (i.e., tip expands and hub contracts) if the blade operates at an area ratio that is below the choke limit line at negative incidence.

The radial variation in streamtube area ratio for the three sizes of perturbation applied is shown in Fig. 25, where the spanwise redistribution up to the throat is included. There is, as expected, a continuous variation up the span of the blade whose magnitude increases with the velocity perturbation.

Figure 26 shows the streamwise development of the radial contractions at the hub, mid-section, and casing for a constant 5% velocity perturbation applied to inlet mean Mach numbers between 0.30 and 0.90. There are two important points to note. First, the effect is highly Mach number dependent, increasing rapidly as the Mach number approaches one. Second, the radial redistribution starts upstream of the blade leading edge and continues downstream of the blade trailing edge. Half of the contraction occurs upstream of the throat and half downstream.

The fact that half the contraction occurs upstream of the throat and half downstream agrees with the work of Hawthorne and Ringrose [9] and Horlock [10] on compressible actuator disk theory. Horlock states that in the actuator disc theory, this occurs because the contraction is created by vorticity produced at the disc. The potential field created by this vorticity results in exactly half the contraction occurring upstream of the disc and half downstream.

The transonic relief mechanism is important because it essentially gets the blade "out of trouble." Whether the issue is bad design, manufacturing variation, or an incorrect inlet incidence (as will be shown in Sec. 4.4), transonic relief acts to move the blade toward the unique optimal area ratio.

4.3 Physical Mechanism. The vorticity at the inlet of a real fan or compressor depends on its location within the engine. A first stage fan draws air from the environment with zero vorticity

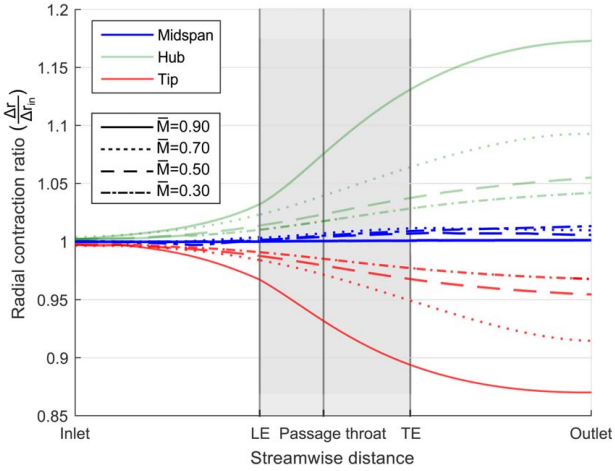

Fig. 26 Streamtube contraction ratio for a velocity perturbation of 5% across the blade passage at an average inlet Mach number of 0.30, 0.50, 0.70, and 0.90

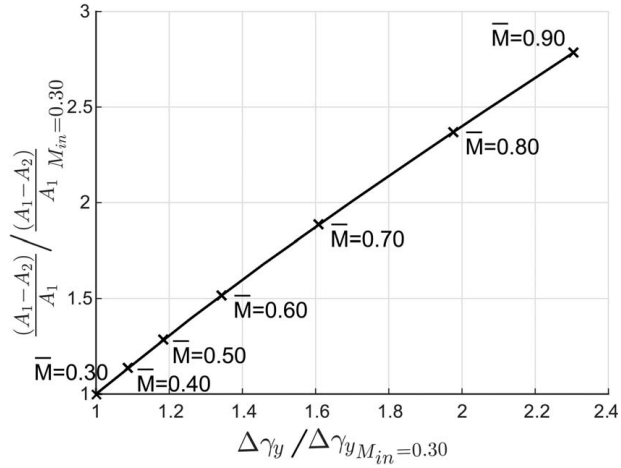

Fig. 28 Relationship between area ratio of the upper stream and the change in pitchwise vorticity across the blade row

in the absolute frame. In the blade relative frame, the inlet flow therefore only has an axial component of vorticity. The vorticity composition at the inlet of an embedded stage is more complex due to spanwise variations in axial velocity.

The simple model used in this study is shown in Fig. 27. The figure depicts an idealized version of the simple model used in the 3D CFD earlier. At the inlet to the blade row, the sharp change in velocity is now represented by an equivalent vortex sheet of strength γ. In the model, the vorticity is assumed to be normal to the streamwise direction at the blade inlet. Figure 27 shows the pitchwise component of this vorticity.

Because the vorticity at the inlet of the simple model is normal to the streamwise direction, it is a special case of the more general case found in compressors and fans. However, the same physical mechanism is at work and the simple model has the virtue of allowing the transonic relief to be decoupled from other effects. In Sec. 5, we will return to the case of a first stage fan and demonstrate that the same mechanism occurs.

Any mass redistribution across the blade row must correspond to a change in the strength of the pitchwise vorticity between the inlet and the exit of the blade. Figure 28 plots the relationship between the change in pitchwise vorticity and the change in the area ratio predicted by the CFD. This clearly shows that for transonic relief to occur, there must be an increase in the magnitude of pitchwise vorticity across the blade row.

Marsh [11] studied the effect of Mach number on the vorticity produced by a cascade of blades. His method was based on applying Kelvin's circulation theorem to compressible flow through a cascade. Following Hawthorne [12], he broke down the change in vorticity across the blade row into the two mechanisms shown in Fig. 29. The first, Fig. 29(*a*), is the trailing shed vorticity, $\gamma_{s(shed)}$, which is caused by the variation of circulation along the span of the blades. This is a result of the variation in velocity and Mach number up the span of the blade at inlet changing the spanwise lift distribution. The second component, Fig. 29(*b*), is the vorticity created by the stretching of the inlet vortex filaments as they pass through the blade row.

The stretching of the inlet vortex filament as it passes through the blade row, shown in Fig. 29(*b*), results in two vorticity components. One component is distributed in the flow $\gamma_{(dist)}$, while the other is a vortex filament in the wake leaving the blade trailing edge $\gamma_{(fil)}$. The component distributed in the flow has both a streamwise component, $\gamma_{s(dist)}$, and a normal component, $\gamma_{n(dist)}$, while the vortex filament leaving the blade trailing edge has only a streamwise component, $\gamma_{s(fil)}$. This stretching of the inlet vortex filament is a direct result of the difference in the time it takes for a particle to travel over the blade's suction and pressure surface, known as residence time.

Marsh [11] developed an analytical method for predicting how the aforementioned components of vorticity depend on the Mach number. Figure 30 illustrates how the increase in pitchwise vorticity across the blade row varies with the Mach number. The shaded regions are the CFD predictions, and the lines with crosses are the predictions using Marsh's method.

Marsh's method provides a relationship for the change in the normal component of vorticity γ_n across the blade row:

$$\gamma_{n_2} = \left[\frac{V_1}{V_2}\frac{T_2}{T_1}\right]\gamma_{n_1} = \frac{\mathrm{M}_1}{\mathrm{M}_2}\left[\frac{1+\frac{(\gamma-1)}{2}\mathrm{M}_1^2}{1+\frac{(\gamma-1)}{2}\mathrm{M}_2^2}\right]^{\frac{1}{2}}\gamma_{n_1} \tag{3}$$

This expression shows that as the Mach number rises so does the increase in normal vorticity $\Delta\gamma_n$. From Fig. 30, it is clear that

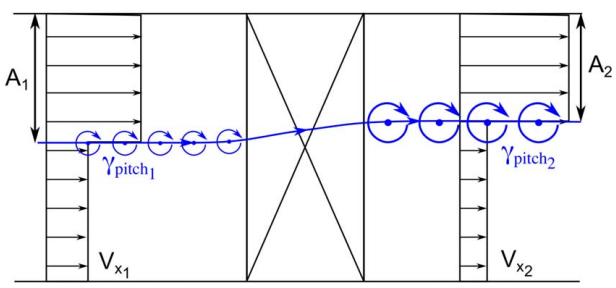

Fig. 27 Physical mechanism responsible for transonic relief

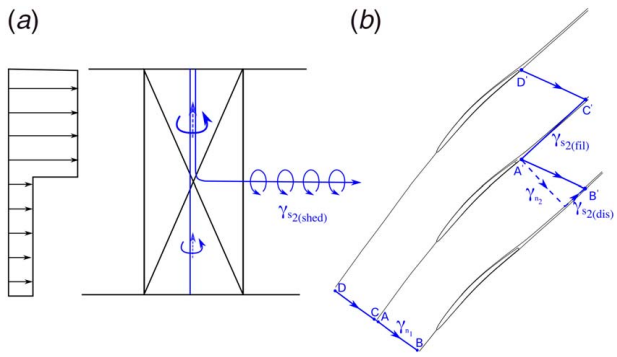

Fig. 29 (*a*) Trailing shed vortex filament and (*b*) stretching of inlet vortex filament in blade row

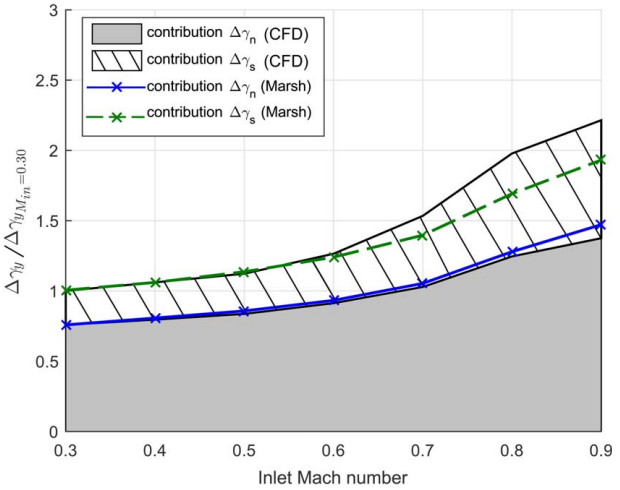

Fig. 30 Increase in pitchwise vorticity with Mach number predicted by CFD and Marsh [11]

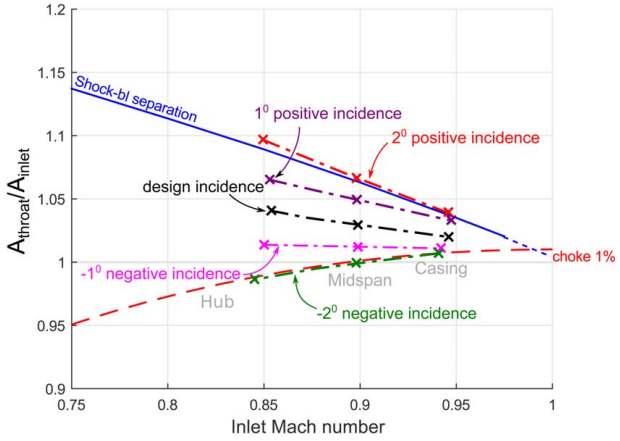

Fig. 31 Effect of incidence change on transonic relief

Marsh's method and the CFD are in good agreement.

Marsh's method does not provide a direct relationship for the change in the streamwise component of vorticity across the blade row $\Delta\gamma_s$. However, it does show that it is directly dependent on the secondary velocities at the exit to the blade passage induced by $\gamma_{s(dist)}$. Under the conservative assumption that $\Delta\gamma_s$ varies proportionally with the change in $\Delta\gamma_{s(dist)}$, a relationship can be written for the variation of $\Delta\gamma_s$ with Mach number in the limit where the cascade turning is small:

$$\frac{(\Delta\gamma_s)}{(\Delta\gamma_s)_{inc}} = 1 + \frac{(\gamma - 1)}{2} M_1^2 \tag{4}$$

where $(\Delta\gamma_s)_{inc}$ is the change in streamwise vorticity for an incompressible flow.

The green line with crosses was plotted using the expression derived in Eq. (4) adjusted for a representative flow turning as described by Marsh [11]. $(\Delta\gamma_s)_{inc}$ was derived from the CFD solution at an inlet Mach number of 0.30.

It is evident from Fig. 30 that although the agreement between Marsh's method and the CFD is not as good as for the normal vorticity, it still predicts the rise in streamwise vorticity with Mach number with relative accuracy, thus capturing the underlying physics.

The good overall agreement between Marsh's method and the CFD indicates that the variation of transonic relief with Mach number is correctly predicted by applying Kelvin's circulation theorem for compressible flow through a cascade.

4.4 Varying Incidence. Figure 31 shows the effect of incidence on the variation of A_{throat}/A_{inlet} across the blade span. The mid-span variation in A_{throat}/A_{inlet} is simply caused by the change in A_{inlet} as the incidence changes. The effect of transonic relief causes the gradient in the variation in A_{throat}/A_{inlet} across the blade span to change. It can be deduced that as incidence is increased, the transonic relief mechanism strengthens, increasing the gradient in the variation of A_{throat}/A_{inlet}. It can also be seen that as incidence becomes negative, the transonic relief mechanism first weakens and close to choke the gradient switches sign. This means that the area ratio of the high Mach number streamtube expands rather than contracts.

Over the entire incidence range, transonic relief can be seen to always move A_{throat}/A_{inlet}, of the streamtube with the highest inlet Mach number, toward its optimum value of 1.01. This is a very powerful effect because it allows each streamtube to self-adjust to ensure that the blade remains unchoked and unseparated. Without this mechanism, transonic blade rows would have no operating incidence range.

Figure 32 shows the effect of incidence on the increase in the pitchwise component of vorticity, across the blade row. It includes both the prediction using the method developed by Marsh and the CFD prediction. Once again, the method developed by Marsh accurately predicts the change in vorticity across the cascade. It should be noted that at the lowest incidence, −2 deg incidence, i.e., close to the choke limit, the magnitude of transonic relief predicted by the CFD deviates further from the Marsh prediction. This occurs due to significant entropy changes along the blade span, which are not taken into account in Marsh's method [11]. It is interesting to note that this increase in entropy across the blade row acts to amplify the effect of transonic relief.

5 Engine Representative Case

It is important at this point to demonstrate transonic relief in an engine representative case. The case chosen is a transonic fan, which draws air of zero vorticity from a large plenum. The fan was designed with a hub-to-tip ratio of 0.75 and an aspect ratio of 2.0. The inlet blade angle is of a free-vortex design, and the loading distribution up the span is engine representative. The inlet profiles to the transonic compressor rotor are shown in Fig. 33. For clarity, the calculation was performed with no hade and no tip gap, and the endwall was modeled as a slip surface. The gray dashed line in Fig. 34 shows the variation in A_{throat}/A_{inlet} across the blade span. The tip value of the area ratio was deliberately set too high at $A_{throat}/A_{inlet} = 1.05$. This would cause the suction surface of the tip section of the blade to be separated by a strong shock.

The black dashed line in Fig. 34 shows the variation of A_{throat}/A_{inlet}, at design incidence, extracted from the CFD. A_{throat}/A_{inlet} in the tip section was found to have decreased to a value of 1.01, which is the optimal value. Though the primary mechanism responsible for this change is likely transonic relief, it is not possible to decouple it from the effect of the spanwise variation in density due to radial equilibrium and the spanwise variation in blade design up the span. This occurs as the blade row is of finite radius.

A better demonstration of transonic relief is the effect of changing the blade's mean incidence on A_{throat}/A_{inlet}. The effects of positive and negative incidences are depicted by the red and green dashed lines, respectively, in Fig. 34. For these cases, the spanwise distribution of density remains unchanged across the span as does the blade geometry. Therefore, any changes in A_{throat}/A_{inlet} are primarily caused by the mechanism of transonic relief. As observed previously, as incidence is increased, the variation of A_{throat}/A_{inlet} with inlet Mach number rotates in a clockwise direction. As the incidence is decreased and turns negative, the variation of A_{throat}/A_{inlet} with inlet Mach number rotates in an anti-clockwise direction.

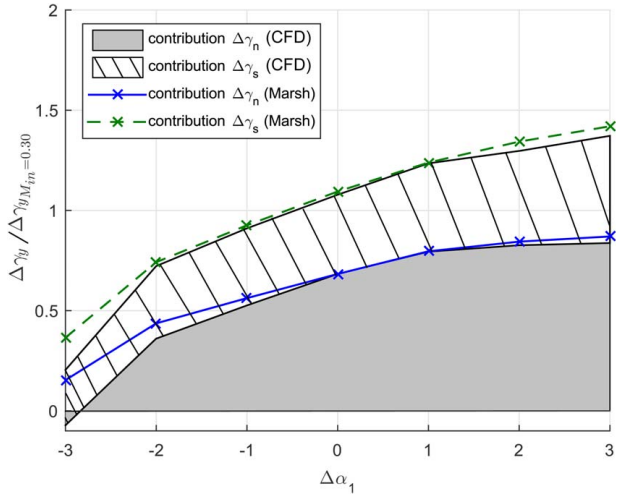

Fig. 32 Increase in pitchwise vorticity with varying incidence predicted by CFD and Marsh [11]

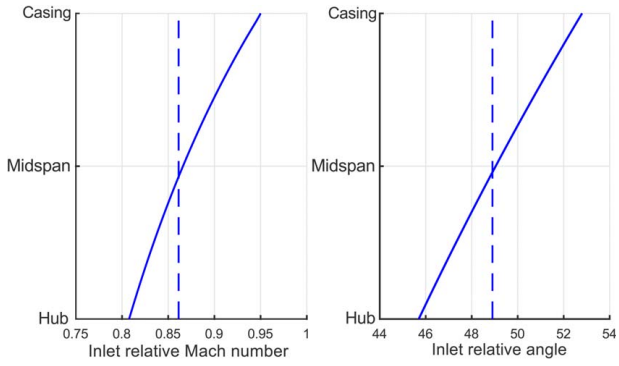

Fig. 33 Inlet profiles for an engine representative transonic compressor (casing Mach number 0.95)

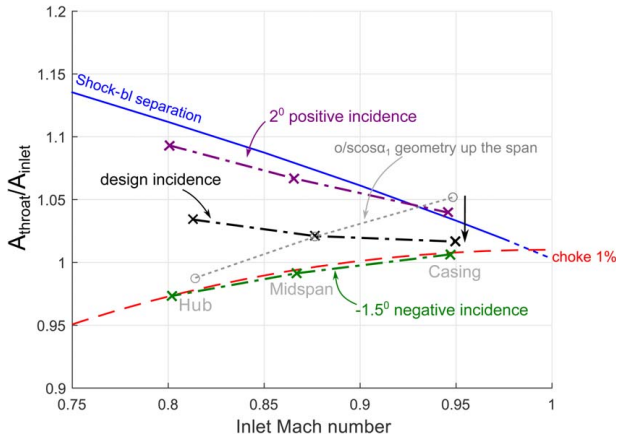

Fig. 34 Spanwise variation in streamtube area ratio in an engine representative transonic compressor

Most importantly, in both cases, the effect of transonic relief is to move the A_{throat}/A_{inlet} toward its optimal value, $A_{throat}/A_{inlet} = 1.01$.

Figure 35 plots the relationship between the change in pitchwise/tangential vorticity and the change in the area ratio predicted by the CFD. The figure shows that, in a similar way to the simple model, transonic relief alters the area of the streamtube by changing the difference in the pitchwise component of vorticity across the blade row.

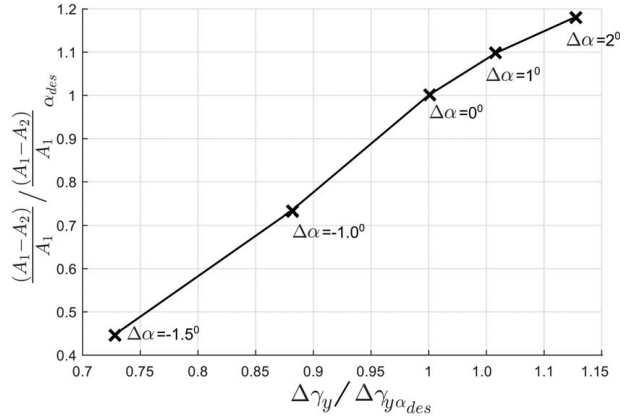

Fig. 35 Relationship between area ratio of the casing streamtube and the change in pitchwise vorticity across the blade row

6 Application to Preliminary Design

In early-stage design, one-dimensional preliminary design systems are used to predict the operating characteristic of high-speed compressors. These methods rely on the operating incidence range of each blade row being known. This article has shown that the operating incidence range of a transonic blade row is highly dependent on the strength of the transonic relief mechanism. A method of incorporating transonic relief into the preliminary design will therefore be demonstrated.

Based on the principles of transonic relief presented in this article, two key parameters control the strength of this mechanism. These are the relative tip Mach number (M_{tip}) and the difference in relative spanwise Mach number from hub to tip (ΔM), which can be controlled by the hub-to-tip ratio or the inlet swirl profile in a multistage machine. For a fixed M_{tip}, the larger ΔM is, the stronger the transonic relief mechanism will be.

Figure 36 shows the universal plot of incidence range of a blade row plotted as a function of M_{tip} and ΔM. The incidence range is defined by a 20% increase in loss relative to that at design incidence. Each datapoint in Fig. 36 is from a CFD solution of a compressor designed with a different hub-to-tip ratio and different tip Mach number. The design of each compressor was undertaken in the same way as described in Sec. 5; with each blade section up the span designed at the optimal area ratio based on Eq. (2) after accounting for the true $AVDR_{throat}$. The lines of best fit are also presented for each tip Mach number case studied.

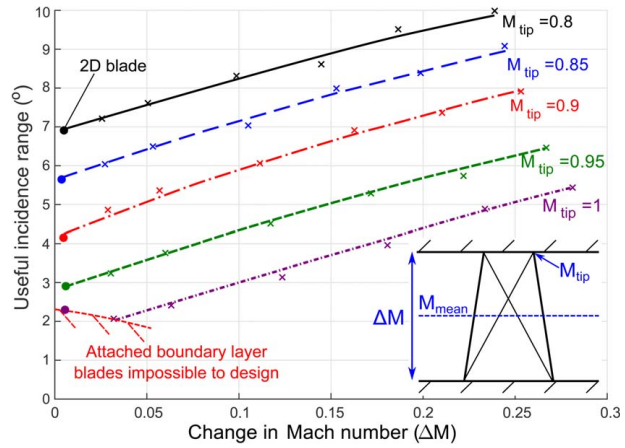

Fig. 36 Universal relationship between useful incidence range and change in spanwise Mach number for different tip Mach numbers up to sonic

It is interesting to note the red hashed region in the bottom left of Fig. 36 where design is impossible. This is the region, discussed in Sec. 3.6, where the transonic relief mechanism is too weak to allow a blade with an inlet Mach number of one to operate without it being simultaneously choked and its suction surface being separated by a shock. This shows that in such a case, by reducing the hub-to-tip ratio, the change in Mach number across the span would rise and the design could be successfully realized.

Figure 36 can be used in a preliminary design system to allow the incidence range of each blade row to be determined. To highlight the importance of capturing this mechanism at the preliminary design stage, consider the case where a designer is trying to select a tip Mach number for a blade with a fixed mean inlet Mach number (M_{mean}). In practice, the tip Mach number can be controlled by changing either the hub-to-tip ratio or inlet swirl distribution in the multistage environment. A designer might be hesitant to go to a lower hub-to-tip ratio machine or have a more uniform inlet swirl because the tip Mach number would be pushed up. However, in addition to an increase in M_{tip}, ΔM also increases. Figure 36 shows that these two actions have the opposite effect on a blade's incidence range and in many cases are equal and opposite and therefore cancel. This means that although M_{tip} increase, there is effectively no change in the blade row's incidence range.

7 Conclusions

It has been demonstrated that as the inlet Mach number approaches unity, the key design parameter is the area ratio between the blade throat area and the upstream passage area and that only one unique value exists at the sonic condition ($A_{throat}/A_{inlet} = 1.01$). This occurs as at higher area ratios, the suction surface of the blade is separated by a strong shock, while at lower area ratios, the blade is choked.

In terms of two-dimensional or quasi-three-dimensional design, a new correlation for specifying A_{throat}/A_{inlet} during the preliminary design process has been developed. In addition, it has been shown that the pitch-to-chord of the transonic blades has a relatively weak effect on the blade's operating range and design performance. As a result, this is a useful degree-of-freedom for the designers of transonic and supersonic blade rows.

The practical design of fans and compressors is only possible because of the mechanism of transonic relief. This mechanism has been demonstrated to self-adjust the spanwise height of the sonic streamtube, always moving A_{throat}/A_{inlet} toward its optimal value of 1.01. This leads to the conclusion that if during design, manufacture, or off-design operation, A_{throat}/A_{inlet} is nonoptimal, then transonic relief will act to self-correct its value within the acceptable operating range.

Furthermore, the physical mechanism responsible for transonic relief has been identified as the change in the pitchwise component of vorticity across the blade row. This is caused by both the shed lift and the distortion of inlet vorticity through the blade row. Using Kelvin's circulation theorem applied to compressible cascade flow and CFD, it has been shown that the change in pitchwise vorticity strongly amplifies with the increasing inlet Mach number and spanwise change in Mach number.

The exploitation of transonic relief has a number of significant implications. First, during the manufacture of transonic compressor and fan blades, geometric tolerances are usually set to be very small. This work has shown that the most important parameter for the operation of a transonic blade is A_{throat}/A_{inlet}. However, it has also been shown that transonic relief acts to self-correct for any manufacturing errors in A_{throat}/A_{inlet}. This implies that it might be possible to relax geometric tolerances on the manufacture of transonic blading. Future work should be undertaken to investigate this.

Second, it implies that transonic compressors with a high hub-to-tip ratio are likely to be nearly impossible to design. Such compressors only have a small variation in inlet Mach number over the blade span. This means that the effect of transonic relief will be relatively weak, making blade design inherently more difficult. This article presents a universal low-order relationship that can be used in the preliminary design of core compressors linking useful mean incidence range to important blade design features, such as the hub-to-tip ratio.

Finally, transonic relief is very likely to also be of benefit in the design of distortion tolerant transonic fans for future propulsion systems and boundary layer ingestion fans. This is because transonic relief has a similar effect on circumferential annular distortions as it has for the spanwise distortions presented in this article.

Acknowledgment

The authors would like to thank Rolls-Royce plc for their support and permission to publish this work and the EPSRC for their support (DTP award). A special thanks is extended to Professor Nick Cumpsty for his direct involvement and for instigating many of the ideas presented in this article; as well as Chris Hall, Mark Wilson, Simon Gallimore, and Bronwyn Power for their invaluable advice, many discussions and feedback on the results. Finally, we would like to thank the Compressor Group at the Whittle Laboratory; especially James Taylor and Tony Dickens.

Conflict of Interest

There are no conflicts of interest.

Data Availability Statement

The datasets generated and supporting the findings of this article are obtainable from the corresponding author upon reasonable request. The authors attest that all data for this study are included in the paper. Data provided by a third party listed in Acknowledgment. No data, models, or code were generated or used for this paper.

Nomenclature

c	=	chord
o	=	2D section minimum passage length
r	=	radius
s	=	pitch
A	=	area
P	=	pressure
V	=	velocity
Y_p	=	profile loss coefficient: $\Delta p_0/(p_{0inlet}—p_{inlet})$
y^+	=	dimensionless wall distance
bl	=	boundary layer
ss/sb	=	supersonic/subsonic
M/M_{in}	=	Mach number/inlet Mach number
Tu	=	turbulence intensity
1D/2D/3D	=	one/two/three dimensional
α	=	flow angle measured from axial
γ	=	vortex sheet strength
$\Delta\alpha$	=	$\alpha - \alpha_{des}$
ρ	=	density

Subscripts

des	=	at design incidence
is	=	isentropic
n/s	=	normal/streamwise quantity
neg/pos	=	evaluated at negative/positive incidence
o	=	stagnation quantity
rel	=	relative frame
x/y	=	axial/pitchwise quantity
1/2	=	evaluated at blade row inlet/exit

References

[1] McKenzie, A. B., 1997, *Axial Flow Fans and Compressors: Aerodynamic Design and Performance*, Ashgate Publishing, UK.

[2] Cumpsty, N. A., 2004, *Compressor Aerodynamics*, Krieger Publishing, Malabar, FL.

[3] Ginder, R. B., and Calvert, W. J., 1987, "Design of an Advanced Civil Fan Rotor," ASME J. Turbomach., **109**(3), pp. 340–345.

[4] Wright, P. I., and Miller, D. C., 1981, "An Improved Compressor Performance Prediction Model," Institution of Mechanical Engineers European Conference, Mar. 19–20, Paper No. C423/028.

[5] Drela, M., and Youngren, H., 1998, *A User's Guide to MISES 2.53*, Massachusetts Institute of Technology, Cambridge, MA.

[6] Kusters, B., Schreiber, H. A., Koller, U., and Monig, R., 1999, "Development of Advanced Compressor Airfoils for Heavy Duty Gas Turbines—Part II: Experimental and Analytical Analysis," ASME J. Turbomach, **122**(3), pp. 406–414.

[7] Brandvik, T., and Pullan, G., 2010, "An Accelerated 3D Navier Stokes Solver for Flows in Turbomachines," ASME J. Turbomach, **133**(2), p. 021025.

[8] Spalart, P., and Allmaras, S., 1992, "A One Equation Turbulence Model for Aerodynamic Flows," AIAA J., **94–439**(1), pp. 5–21.

[9] Hawthorne, W. R., and Ringrose, J., 1964, "Actuator Disc Theory of the Compressible Flow in Free-Vortex Turbomachinery," Proc. Inst. Mech. Eng., **178**(Pt. 3I(ii)), pp. 1–13.

[10] Horlock, J. H., 1980, "Choking Effects in Blade Rows of Turbomachines," J. Mech. Eng. Sci., **22**(4), pp. 161–173.

[11] Marsh, H., 1975, "Secondary Flow in Cascades—The Effect of Compressibility," Aeronautical Research Council Reports & Memoranda, **No. 3778**, pp. 1–32.

[12] Hawthorne, W. R., 1955, "Rotational Flow Through Cascades, Pt. 1, The Components of Vorticity," Q. J. Mech. Appl. Math., **8**(Pt. 3), pp. 266–279.